Published in final edited form as:
Am J Physiol Heart Circ Physiol. 2005 March ; 288(3): H1113–H1123. doi:10.1152/ajpheart.00882.2004.

Dynamic model for ventricular junctional conductance during the cardiac action potential

Xianming Lin[1], **Joanna Gemel**[2], **Eric C. Beyer**[2], and **Richard D. Veenstra**[1]

[1]Department of Pharmacology, State University of New York Upstate Medical University, Syracuse, New York

[2]Department of Pediatrics, University of Chicago, Chicago, Illinois

Abstract

The ventricular action potential was applied to paired neonatal murine ventricular myocytes in the dual whole cell configuration. During peak action potential voltages >100 mV, junctional conductance (g_j) declined by 50%. This transjunctional voltage (V_j)-dependent inactivation exhibited two time constants that became progressively faster with increasing V_j. G_j returned to initial peak values during action potential repolarization and even exceeded peak g_j values during the final 5% of repolarization. This facilitation of g_j was observed <30 mV during linearly decreasing V_j ramps. The same behavior was observed in ensemble averages of individual gap junction channels with unitary conductances of 100 pS or lower. Immunohistochemical fluorescent micrographs and immunoblots detect prominent amounts of connexin (Cx)43 and lesser amounts of Cx40 and Cx45 proteins in cultured ventricular myocytes. The time dependence of the g_j curves and channel conductances are consistent with the properties of predominantly homomeric Cx43 gap junction channels. A mathematical model depicting two inactivation and two recovery phases accurately predicts the ventricular g_j curves at different rates of stimulation and repolarization. Functional differences are apparent between ventricular myocytes and Cx43-transfected N2a cell gap junctions that may result from posttranslational modification. These observations suggest that gap junctions may play a role in the development of conduction block and the genesis and propagation of triggered arrhythmias under conditions of slowed conduction (<10 cm/s).

Keywords

gap junctions; connexin43; voltage gating; inactivation; kinetics; repolarization

Cardiac gap junctions provide for rapid transmission of the cardiac action potential via intercellular ionic currents among all cardiac cell types. In the mammalian heart, connexin40 (Cx40), connexin43 (Cx43), and connexin45 (Cx45) are all expressed in varying amounts and distributions (16,31). In the adult myocardium, Cx40 is found primarily in the atrium, His-Purkinje, and sinoatrial (SAN) and atrioventricular (AVN) nodes, whereas Cx43 is found in the working myocardium of the atrium and ventricle and in the more distal regions of the Purkinje network (2,10,11,15,28). Cx45 is expressed in the highest amounts during the second trimester of development, and its role in the adult myocardium is restricted to the SAN, AVN, and ventricular conduction system, with only trace amounts remaining in the working myocardium (1,3,6,7). There is some speculation about the role of Cx45 in the ventricular

Address for reprint requests and other correspondence: R. D. Veenstra, Dept. of Pharmacology, SUNY Upstate Medical Univ., 750 East Adams St., Syracuse, NY 13210 (veenstrr@upstate.edu).

myocardium emanating from its low level of expression and the maintenance of action potential propagation in animal models of Cx43-deficient hearts (14,42).

Increases in gap junctional resistance (r_j) can produce heterogeneities in action potential duration and conduction velocity (θ). These nonuniformities in gap junctional conductance may be the result of heterogenous expression of Cx43 or the result of local environmental factors, such as hypoxia, acidosis, and hyperkalemia that occur during ischemia (29). Gap junction remodeling after ischemia, infarction, or hypertrophy reduces or terminates the intercellular transfer of ionic current via gap junction channels and contributes to arrhythmogenesis (5,17,23,26,27,43). Slow conduction is associated with arrhythmias resulting from reentrant excitation. Decreases in membrane excitability can cause reductions in θ from 50 to 17 cm/s before conduction block ensues, whereas increases in r_j can produce θ as low as 0.26 cm/s before conduction failure occurs (34). Below a θ of 10 cm/s, the intercellular conduction delay is sufficient to produce transjunctional voltage gradients (V_j) equal to the amplitude of the cardiac action potential (22). In our previous studies, we demonstrated that V_j gradients equal to the amplitude of the ventricular cardiac action potential produce time-dependent changes in junctional conductance (g_j) in Cx43 and Cx40 gap junctions (21,22). Inactivation of g_j by as much as 60% occurred predominantly at V_j >100 mV and recovered to peak values during the repolarization phases of the action potential.

In this study, we directly measured the changes in g_j between cultured neonatal mouse ventricular myocyte pairs while experiencing V_j gradients equivalent to the amplitude of a ventricular cardiac action potential at six different rates of simulation. We demonstrate qualitatively similar results to those we obtained from stable clones of rat Cx43-transfected murine neuro2a (N2a) neuroblastoma cells. We further demonstrate that inactivation and recovery are distinct processes with different steady-state Boltzmann distributions. The most notable observation was an increase in g_j above peak values during final repolarization that occurred only in ventricular myocyte gap junctions. The quantitative differences between the two preparations are defined in the context of a “dynamic” cardiac gap junction model designed to accurately describe the time-dependent changes in g_j experienced during the normal ventricular action potential and during prolonged repolarization. These quantitative differences in function do not likely result from the expression of Cx40 and Cx45, since their content was mimimal in 2-day cultured ventricular myocytes.

Materials and Methods

Myocyte cell culture

The torsos from freshly killed newborn C3H or C57BL6 mice [Jackson Laboratory, Bar Harbor, ME; courtesy of Dr. Paul Massa, Dept. of Neurology, State University of New York (SUNY) Upstate Medical University, Syracuse, NY] were collected for extirpation of the heart. The newborn mice were killed in accordance with approved methods by the institution's Committee for the Humane Use of Animals. The excised hearts were placed in ice-cold Ca^{2+}- and Mg^{2+}-free Hanks' balanced salt solution (CMF HBSS; Worthington Biochemical, Lakewood, NJ) or DMS8 (in mM: 116 NaCl, 5.4 KCl, 1.0 NaH_2PO_4, and 5.5 dextrose; see Ref. 36). The atria and ventricles were separated and placed in 35-mm petri dishes containing 3 ml of ice-cold buffer, minced by three to five cuts with a fresh scalpel blade, and placed in a 25-ml Erlenmeyer flask containing 5 ml enzymatic dissociation medium. The trypsin dissociation medium contained 0.05% trypsin (3× crystallized; Worthington) and 75 U/ml purified collagenase (Worthington) dissolved in CMF HBSS. The collagenase dissociation medium contained 2 mg/ml collagenase (type 2; Worthington), 5.5 μg/ml DNase I (Worthington), and 1 mg/ml BSA (fraction V; Sigma Chemical, St. Louis, MO) dissolved in DMS8 (39). The supernatent from each 10-min dissociation cycle was filtered through a 70-μm cell strainer (Falcon, Franklin Lakes, NJ) in 10 ml L-15 or medium-199 cell culture media

supplemented with 10% FBS and 100 U/ml penicillin-streptomycin (Invitrogen, Grand Island, NY). After the fourth dissociation cycle at 37°C, the remaining tissue was triturated by gentle pipeting and strained, and the cell suspension was pelleted by centrifugation at 500 *g* for 10 min. The pellet was resuspended in 10 ml culture media and enriched for myocytes by 20 min of differential cell adhesion at 37°C in a 100-mm culture dish. The supernatent was pelleted by centrifugation, resuspended in 5 ml culture media, and plated in 35-mm culture dishes for electrophysiological examination 24–72 h later.

Electrophysiology

Whole cell gap junction currents were recorded during repeated voltage-clamp pulses with ventricular action potential waveforms, as previously described (21). TTX (30 μM; Sigma) was added to the bath saline of each dish to prevent activation of the sodium current during the experiments. *Phase 3* repolarization was increased in duration in one set of experiments by increasing the duration of each voltage step (*dt*) from 1.0 to 1.5, 2.0, 3.0, 4.0, and 5.0 ms. Quantitative junctional voltage correction methods were used to correct for series resistance errors resulting from each patch electrode according to the expression (40):

$$g_j = \frac{-\Delta I_2}{V_1 - (I_1 \cdot R_{e11}) - V_2 + (I_2 \cdot R_{e12})} \quad (1)$$

A steady-state junctional current (I_j)-V_j relationship was obtained for each experiment, and the maximum junctional conductance ($g_{j,max}$) was calculated from the slope of the linear regression fit of the −5 to −25 mV I_j-V_j curve for each experiment. The g_j was normalized to this maximum slope conductance value ($G_j = g_j/g_{j,max}$), and the corresponding I_j-V_j relationships [$=I_j/(g_{j,max} \times V_j)$] were calculated according to each experimental $g_{j,max}$ value. The data from three to eight experiments were pooled for each experimental group.

The steady-state V_j-dependent inactivation (increasing V_j) and recovery (decreasing V_j) curves were obtained using the voltage-clamp protocol depicted in Fig. 1. A 200 ms/mV voltage ramp from −40 to −160 mV was followed by the reverse progression of the command voltage applied to (prejunctional) *cell 1* (*trace 1*). After a 24-s rest period, the polarity of the voltage ramp was reversed to proceed from −40 to +80 mV and back again (*trace 2*). The whole cell current traces in Fig. 1 show the hysteresis observed between the inactivation and recovery processes during one experiment from a pair of ventricular myocytes. The ensemble average of five complete traces was complied from each ventricular cell pair for determination of the steady-state inactivation and recovery curves. The steady-state inactivation and recovery curves were independently fit with the Boltzmann equation:

$$G_j^{SS} = \left(\frac{G_{ss}^{max} \cdot \left\{ \exp\left[A \cdot \left(V_j - V_{1/2} \right) \right] \right\} + G_{ss}^{max}}{1 + \left\{ \exp\left[A \cdot \left(V_j - V_{1/2} \right) \right] \right\}} \right) \quad (2)$$

where G_{ss}^{min} is 1($G_j = g_j/g_{j,max}$) = the resting normalized slope conductance between ±5 and ±25 mV for each experiment, G_{ss}^{min} is the minimum value of $g_j/g_{j,max}$, A is the slope factor for the Boltzmann curve {$=zF/RT$ at 20°C, where z is the valence in elementary charge units (q), F is Faraday's constant (in coulombs/mol), R is the molar gas constant [in J/(mol·K)], T is temperature (in K)}, and $V_{1/2}$ is the half-inactivation voltage. Curve-fitting procedures were performed using Clampfit software (pCLAMP version 8.2; Axon Instruments) using the sum of squared errors minimization procedure, and the standard error for each estimated parameter

is provided. Final graphs were prepared using Origin version 6.1 or 7.0 software (OriginLab, Northampton, MA).

Immunohistochemistry

The final myocyte suspension was plated in four-well culture slides at a density of 0.5 ml/well and cultured as above. The myocyte cell cultures were fixed with 4% paraformaldehyde at 20° C for 15 min, permeabilized, blocked, and incubated overnight at 4°C with primary connexin-specific antibodies according to the procedures of Kwong et al. (20). Ventricular myocytes were stained using a rabbit anti-Cx40 or rabbit anti-Cx45 polyclonal antibody (1:100 dilution) and a mouse anti-Cx43 monoclonal antibody (1:150 dilution; Zymed Laboratories, San Francisco, CA, or Chemicon International, Temecula, CA). The cells were labeled with goat Alexa Fluor488 anti-rabbit or goat Alexa Fluor546 anti-mouse secondary antibodies (1:1,500 dilution) for 3 h at room temperature (Molecular Probes, Eugene, OR). Coverslips were mounted on the dried slides using the Prolong antifade medium and reagent (Molecular Probes).

Photomicrographs were acquired using a Zeiss Axiovert microscope (Carl Zeiss, Munich, Germany) under Xenon epifluorescent illumination using a Cy2 or Cy3 excitation/emission filter cube using Micromorph software (version 1.4 for Windows; CMM, Paris, France). Exposure times were 5.0 or 6.5 s for Cx40 and Cx45 at an excitation wavelength of 484 nm and 1.0 s at 555 nm for Cx43 at ×40 magnification (courtesy of Dr. David Cameron, Dept. of Neuroscience and Physiology, SUNY Upstate Medical University).

Immunoblot analysis

Parental N2a cells, HEK293 cells, or stable transfected rat Cx40 or Cx43 N2a cells were harvested from T-75 flasks by scraping in the presence of 2 mM ice-cold phenylmethylsulfonyl fluoride (PMSF) in PBS. Cultured ventricular myocytes were grown in 100-mM culture dishes for 24–72 h and harvested by scraping in 2 mM PMSF-PBS. The harvested cells were pelleted by centrifugation at 10,000 rpm for 2 min, and the supernatent was discarded, rapidly frozen in liquid nitrogen, and stored at − 80°C until analysis by Western blotting. Fresh frozen ventricular tissue was rinsed in ice-cold HBSS, placed in a 1.5-ml microcentrifuge tube, rapidly frozen in liquid nitrogen, and stored at − 80°C until immunoblot analysis. N2a and HEK293 cells were grown as described previously (8).

Samples were resuspended in 25–100 μl PBS (depending on the size of the sample) containing protease inhibitors (200 μg/ml soybean trypsin inhibitor, 1 mg/ml benzamidine, 1 mg/ml γ-aminocaproic acid, and 2 mM PMSF) and phosphatase inhibitors (20 mM $Na_4P_2O_7$ and 100 mM NaF) and lysed by sonication. The protein concentrations of homogenates were determined using the method of Bradford (4; Bio-Rad, Richmond, CA). Protein samples (50–100 μg) were resolved on 8% polyacrylamide gels containing SDS. Rainbow molecular mass marker standards (Amersham Biosciences) were used to calibrate the gels.

Proteins were electrotransferred from gels on Immobilon-P membranes (Millipore, Bedford, MA) at 300 mA for 1.5 h. Membranes were blocked in 10% nonfat milk in Tris-buffered saline (TBS), pH 7.4, overnight at 4°C and then incubated for 3 h at room temperature with either mouse monoclonal antibodies directed against amino acids 354–367 of human Cx45 (1:1,000 dilution, MAB3100; Chemicon), rabbit polyclonal antibodies directed against amino acids 363-382 of Cx43 (1:4,000 dilution, C6219; Sigma Chemical), or a rabbit antiserum directed against a bacterially expressed Cx40 carboxyl tail fusion protein (1:5,000 dilution; see Ref. 20). After being rinsed repeatedly in TBS, blots were incubated for 1 h at room temperature with peroxidase-conjugated goat anti-rabbit IgG (1:5,000 dilution) or donkey anti-mouse IgG (1:5,000 dilution; Jackson ImmunoResearch Laboratories) used as secondary antibodies. All antibodies were diluted in 10% nonfat milk in TBS, pH 7.4. After being rinsed repeatedly in

TBS, immunoblots were developed with enhanced chemiluminescence (ECL) reagents (Amersham Biosciences).

Results

Connexin expression in murine ventricular myocytes

Immunofluorescent localization and immunoblot analysis of Cx40, Cx43, and Cx45 were performed to determine the molecular composition of the neonatal murine ventricular myocyte gap junctions. The immunohistochemistry was performed on 48- to 72-h cultured ventricular myocytes to closely mimic the electrophysiological recording conditions. Cx43 was readily detectable in paired ventricular myocytes (Fig. 2, B and E), whereas Cx40 (Fig. 2A) and Cx45 (Fig. 2D) were barely detectable, even with 5 to 6.5 times the exposure time for the fluorescence micrographs. What Cx40 and Cx45 that were detectable did colocalize to the same region of the apposed membrane surface as Cx43 (Fig. 2, C and F).

All three connexin proteins were readily detectable from fresh frozen neonatal ventricular tissue samples as shown in Fig. 2G, lane 4. Considerably less Cx40 and Cx45 is present in these samples, despite 10 times more protein being loaded in these two lanes relative to the Cx43 lane. This suggests that Cx40 and Cx45 comprise <5% of the total connexin protein in the neonatal ventricle. In contrast to the abundant level of Cx43 in the cultured ventricular myocytes (Fig. 2G, *lane 3*), Cx40 and Cx45 are barely detectable. As a positive control, stable rat Cx40- and Cx43-transfected N2a cells were probed with the same antibodies. These are the same N2a cell clones previously described using the ventricular action potential voltage clamp (21,22). There were no stable Cx45-transfected N2a cells available to use as a positive control, so we used HEK293 cells instead. At least two bands of Cx40 and Cx43 protein were detectable in transfected N2a cells (Fig. 2G, *lane 2*), and there appeared to be less of the higher-molecular-weight Cx43 bands in Cx43-transfected N2a cells (Fig. 2G, *lane 2*) relative to the cultured ventricular myocytes (Fig. 2G, *lane 3*) or fresh frozen tissue (Fig. 2G, *lane 4*). In contrast, there appeared to be less of the lower-molecular-weight band for Cx40 in the frozen ventricular tissue (Fig. 2G, *lane 4*) compared with the Cx40-transfected N2a cell sample (Fig. 2G, *lane 2*). Presumably, these higher-molecular-weight bands are the result of phosphorylation of the regulatory carboxyl terminal domains of the connexins.

Changes in junctional current and conductance during the ventricular action potential

The macroscopic I_j recorded in response to the initial and a train of 100 action potentials at a cycle length (CL) of 1,000 ms is shown Fig. 3A. Comparison with the average applied transjunctional voltage in this same experiment reveals that there is a significant amount of inactivation that occurs during the course of the ventricular action potential. The macroscopic g_j from this same experiment demonstrates that g_j declined from an average peak value of 3.78 to 2.25 nS during the plateau of the action potential (Fig. 3B). It is further revealed that g_j rises during *phase 3* repolarization and attains peak g_j values or higher during the final 5% of repolarization. The average behavior of ventricular myocyte gap junctions ($N = 7$), after normalization to the peak g_j of each experiment, is shown in Fig. 3C. G_j achieves a minimum of 0.50 during the plateau phase and recovers to 1.20 during final repolarization. These same procedures were applied at five other cycle lengths of stimulation, and the average behavior of the ventricular gap junctions at all six frequencies is shown in Fig. 3D. There is slightly less inactivation, only 40% of the peak G_j resulting from the shorter action potential duration, at the higher frequencies of stimulation. G_j recovers to between 1.2 and 1.4 during final repolarization at all frequencies of stimulation.

In a few low g_j experiments, unitary fluctuations in I_j could be observed during successive sweeps of the action potential. One sweep and the ensemble average of all 200 sweeps from

one experiment are displayed in Fig. 3E. The ensemble average of all 200 sweeps at CL = 1,000 ms produces a smooth curve that is indistinguishable from the macroscopic current experiments. Similarly, the conductance calculations for these current records yield very similar results, with an average peak g_j of 130 pS, a minimum g_j of 60 pS, and a maximum final g_j of 240 pS (Fig. 3F). These data are consistent with inactivation and recovery of g_j being the result of the composite V_j gating of no more than five 60-pS gap junction channels during the ventricular action potential.

V_j dependence of inactivation and recovery

To determine the steady-state G_j distributions during increasing and decreasing V_j gradients, the V_j protocol shown in Fig. 1 was applied to four ventricular myocyte cell pairs. The ensemble average I_j was plotted relative to the average V_j from all four experiments in Fig. 4A. For comparison, the same V_j protocol was applied to six Cx43-transfected N2a cell pairs, and the average I_j-V_j relationship is shown Fig. 4D. The arrows indicate the direction of currents during the increasing and decreasing V_j phases of the two I_j-V_j curves. It is apparent from these data that the slope conductance is increased during the return phase only in ventricular myocytes. We have named this process “facilitation” to reflect the apparent opening of more gap junction channels during the decline in V_j than were open at the peak of the ventricular action potential. When g_j is normalized to the peak g_j for all experiments, the G_j-V_j curves for inactivation and recovery are plotted as shown in Fig. 4, B and C, for the ventricular myocytes and Fig. 4, E and F, for Cx43-transfected N2a cells. The solid lines in each panel represent the fitted Boltzmann curves determined using Eq. 2. The parameters for the fitted curves are provided in Table 1. The major differences in the two sets of curves are that the minimum G_j (G_{min}) is higher and the $V_{1/2}$ is smaller in ventricular myocytes relative to Cx43-transfected N2a cells. In both cell types, the gating charge valence and $V_{1/2}$ were reduced during the recovery process, whereas the maximum G_j was higher than initial peak values only in ventricular myocytes.

Kinetics of inactivation

The kinetics of inactivation were determined using a pulse protocol where a V_j pulse of 2.5-s duration was repeated five times and the ensemble average I_j was fitted with an exponentially decaying function to determine the decay time constants. An example of decay time constant fits from one experiment is shown in Fig. 5A. Only the first 400 ms are shown from the −80-, −100-, −120-, and − 140-mV V_j pulses in this example. The reciprocal of the decay time constants from 4 to 10 experiments at each V_j were plotted according to the absolute value of V_j and fitted with the general exponential expression:

$$1/\tau = A^0 \cdot \exp\left[V_j/V_c\,(\mathrm{mV})\right] \tag{3}$$

The rate of inactivation is observed to be an exponential function of V_j with a voltage constant (V_c) of 20.3 ± 0.7 mV and an amplitude at 40 mV (A^0) of 0.00148 ± 0.00024 ms^{-1}. This translates into a rate constant of 675 ms at ±40 mV V_j.

Effects of repolarization on g_j

It is apparent that the declining V_j during the ventricular action potential produces an increase in g_j that was previously demonstrated to be correlated with the two different rates of repolarization (21,22). To examine the effect of prolonged repolarization on the recovery process, the time step of the CL = 1,000 ms ventricular action potential voltage-clamp waveform was increased by 50 to 500% beginning at +85 mV (Fig. 6A). I_j and G_j inactivated by 45–50%, similar to the values observed in Fig. 3 (Fig. 6, B and C). The effect of the longer time step during action potential repolarization is most apparent in Fig. 6D, where G_j is plotted

according to V_j for all six different rates of repolarization. G_j is observed to increase more with increasing duration of phase 3 repolarization. All of the G_j-V_j recovery curves are well described by a two-exponential function, with increasing amplitudes for the higher voltage component as repolarization is prolonged (data not shown).

Modeling rate-dependent changes in G_j

To model the time-dependent G_j curves, a set of equations was derived to calculate the fast and slow inactivation components (G_1^{t+1} and G_2^{t+1}) and the early and late phases of the recovery process (R_1^{t+1} and R_2^{t+1}). The dynamic model for ventricular G_j is defined in the Appendix, and the output of Eq. 11 is illustrated in Fig. 7, A–D, for four of the six cycle lengths. The parameter values for Eqs. 4, 5, 9, and 10 depicting the individual components of the model G_j curves are listed in Table 2. There is essentially no frequency dependence to the model G_j curves, thus indicating that the difference in the shape of the six cycle length curves is the result of the changes in action potential duration associated with different frequencies of stimulation. The changing rates of inactivation were modeled using V_j-dependent decay time constants with a voltage constant equal to the value provided in Fig. 5. The data were best fit by giving the slow inactivation process the initial rate provided by the Eq. 2 fit of the inactivation rates as shown in Fig. 5. The fast inactivation rate was estimated to be six times faster than the slow inactivation. The early recovery phase had an average voltage constant of 25.8 ± 2.4 mV. The late recovery phase, which occurs only in the final 6 mV of repolarization, had a voltage constant of 1.5 mV. The data are well described by the model for all frequencies, and changing the amplitude terms for Eqs. 9a and 10 will modulate the degree of facilitation. The same equations were used to model the prolonged repolarization of the ventricular action potential. The results are shown in Fig. 7, E and F, and the parameter values for the model are listed in Table 3. Only the amplitude and voltage constant were found to vary with increasing duration of the repolarization time step (*dt*). These alterations are conveniently modeled in the Appendix. There was no alteration to the amplitude of the late repolarization phase, which remained a function of the magnitude of facilitation observed during final repolarization.

Discussion

Cardiac excitation involves the generation of an action potential by the integration of a variety of time- and/or voltage-dependent ionic currents present in every cell (18,33). The Luo-Rudy (24,30) model of the ventricular action potential reveals the experimental detail that has gone into understanding the numerous dynamic ionic current components that underlie action potential generation in ventricular myocytes. Cardiac excitation also requires the conduction of the action potential via gap junctions to ensure the rapid, synchronous activation of contraction in the working myocardium, yet there have been few attempts to model the dynamics of cardiac gap junctions and their effect on action potential propagation (13,21,22, 41). In this investigation, we present experimental evidence that ventricular g_j undergoes phasic alterations while experiencing V_j gradients generated by the cardiac action potential (Fig. 3). In agreement with our previous findings on Cx40 and Cx43 gap junctions expressed exogenously in a communication-deficient mammalian cell line, g_j is observed to decline during peak action potential voltages and recover to initial values during action potential repolarization. These phasic changes in g_j are also shown to be the results of the ensemble average of the time- and V_j-dependent gating of individual gap junction channels with unitary conductances (g_j) of 100 pS or less (Fig. 3, E and F). In contrast to our previous findings, we have observed quantitative differences in the rate and magnitude of inactivation experienced during the ventricular action potential and an accentuated increase in g_j as V_j is declining toward resting values that we will subsequently refer to as facilitation. Slow conduction in syncytial myocardium resulting from reduced g_j leads to discontinuous conduction and, paradoxically, an increased safety factor for propagation (18). Intercellular V_j gradients have been

demonstrated under these circumstances, and conduction is expected to be more impaired in a well-coupled syncytium.

The inactivation of ventricular g_j during peak action potential voltages >100 mV relative to the diastolic resting potential occurs with two time constants, similar to what was observed with Cx43 gap junctions expressed in N2a cells (21). Like Cx43, both the fast and slow inactivation time constants had the same V_j dependence. The inactivation rates become *e*-fold faster for every 20.3-mV increase in V_j between ventricular myocytes, similar to the 22.1-mV voltage constant observed for Cx43 (Fig. 5). Of greater functional significance, the slow decay time constant (τ_{slow}) at 40 mV was 2,200 ms for Cx43 compared with 675 ms in ventricular myocytes. The fast time constant was observed to be five times faster than τ_{slow} for Cx43 and six times faster in ventricular myocytes. These observations result in faster inactivation between ventricular myocytes than was observed in Cx43-transfected N2a cells. Despite the faster inactivation at room temperature, the magnitude of inactivation was 10% less in the ventricular myocyte pairs. This difference is also reflected in the G_{min} values of the steady-state inactivation curves for ventricular myocyte gap junctions (0.31–0.37) and Cx43-transfected N2a cells (0.20–0.26; Fig. 4 and Table 1). The steady-state inactivation G_j-V_j relationship also exhibits a 10- to 16-mV lower $V_{1/2}$ and a 0.23–0.40 higher gating charge valence in the native cardiomyocytes compared with homomeric homotypic Cx43 gap junctions. There was little or no frequency dependence to the two inactivation and recovery processes used to define the time-dependent g_j curves at all six test cycle lengths (Fig. 7, A-D, and Table 2). This indicates that g_j is regulated simply by the duration and amplitude of the V_j gradient in existence during the propagating action potential.

Three new findings are reported herein regarding the recovery of g_j during action potential repolarization. First, the steady-state G_j-V_j curve during declining V_j gradients follows a distinct Boltzmann distribution from the frequently described inactivation state G_j-V_j relationship acquired in response to identical but increasing V_j gradients. The $V_{1/2}$ is ~12 mV less during recovery compared with inactivation for both Cx43 and ventricular myocyte gap junctions. Similarly, the gating charge valence was reduced by ~ 1.0 q for ventricular myocytes and 0.5 q for Cx43 during the return from inactivation. This suggests that some charge immobilization has occurred and that gap junction channels reopen by a different process than they close. Second, facilitation occurs only in ventricular myocyte cell pairs. This increase in g_j above initial peak values is not observed only during the final phase of action potential repolarization when vanishingly small V_j gradients can produce large fluctuations in the g_j calculations, but during slow linear V_j ramps of only 1 mV/200 mS. Facilitation can begin as soon as 30 mV during the V_j ramp, in contrast to the final 5% of repolarization during the much faster action potential. These findings are consistent with the previous conclusion that the rate of recovery is determined by the rate of repolarization (21). This concept was further demonstrated by artificially varying the rate of repolarization of the CL = 1,000 ms Luo-Rudy action potential by increasing the time step (*dt*) of the action potential voltage clamp waveform beginning at 85 mV during repolarization (Fig. 7, E and F). Third, the magnitude of the *phase 3* early recovery process increased with increasing duration, and all G_j-V_j curves were well described by double-exponential functions. The apparent recovery time constant for the increasing g_j was indistinguishable from 1 ms (see Appendix and Eq. 9b). Hence, the recovery process was modeled as time independent. The repolarization rate-dependent changes in the amplitude and voltage constant for the early recovery process were modeled based on the values reported in Table 3 (Appendix and Eq. 9b–9d).

The major consequence of prolonging repolarization was to increase the magnitude of the early recovery process during *phase 3* of the action potential. This has possible implications regarding arrhythmogenesis, since early afterdepolarizations (EADs) are triggered during this phase of the action potential and are thought to be the cause of sudden cardiac death associated

with long QT syndromes and other forms of prolonged repolarization. Decreasing g_j widens the "vulnerable window" for the initiation of reentrant excitation by extrasystoles, and computer simulations suggest that intermediate amounts of electrical coupling can facilitate the propagation of EADs (19,32,34). The possible roles of g_j inactivation and facilitated recovery in arrhythmogenesis await further testing in computer models of action potential propagation using the dynamic ventricular gap junction model developed herein. It is conceivable that g_j inactivation promotes orthodromic conduction block and transiently increases anisotropy, whereas g_j recovery promotes the conduction of focal-triggered afterdepolarizations. Facilitation most likely would affect only the generation and propagation of delayed afterdepolarizations, since it occurs only during the final 5% of repolarization. The amount of facilitation is readily altered in the dynamic ventricular g_j model by varying the amplitude of the exponential term in Eq. 10 that defines the late recovery process (R_2^{t+l}).

It is unlikely that the molecular basis for the functional differences in the time- and V_j-dependent changes in g_j between Cx43 and ventricular myocytes is because of the presence of Cx40 and Cx45. Immunohistochemical and immunoblot analysis demonstrate the presence of small amounts of Cx40 and Cx45 in 2-day neonatal murine ventricular myocyte cultures (Fig. 2). This is consistent with previous findings regarding the expression of these three connexins in the ventricular myocardium of the mammalian heart (16,31,38). The observation of two inactivation time constants in macroscopic I_j recordings from paired ventricular myocytes is also consistent with the prevalence of Cx43 gap junction channels. It is also unlikely that the functional differences reflect differences between rat and mouse Cx43, since the two proteins differ by only one amino acid, an asparagine for a serine at position 341 on the carboxyl tail domain of rat and mouse Cx43, respectively (12). One notable difference is that there appears to be more phosphorylated forms of Cx43 in ventricular myocytes relative to Cx43-transfected N2a cells. Cx43 gap junction channels reportedly have three channel conductance (γ_j) states. A 70- to 100-pS state corresponding to the unphosphorylated form (P0), a 40- to 60-pS state corresponding to a monophosphorylated form (P1), and a 20- to 30-pS state corresponding to a double-phosphorylated state of Cx43 are reported to exist (25,35,37). Our immunoblot and γ_j data from transfected N2a cells and murine ventricular myocytes is certainly consistent with the presence of the P0 and P1 forms of Cx43 in both preparations (21). Typically, more phosphorylated Cx43 is observed in native tissues than in transfected mammalian cells (37). It is also possible that accessory association with peripheral membrane proteins (e.g., zona occludens-1) may modulate the function of Cx43 (9,31,36). It was the purpose of this investigation to determine the kinetics for the time- and V_j-dependent changes in ventricular g_j during the action potential and compare them with the like properties of known cardiac connexins. The molecular physiological bases for the two rates of Cx43 inactivation, the facilitation of the recovery process in ventricular myocytes, and the variations in the kinetics and steady-state G_j-V_j relationships remain to be investigated by autonomic neurotransmitters and second messengers and site-directed mutagenesis studies of Cx43.

In conclusion, ventricular gap junctions undergo phasic changes in g_j during the cardiac action potential that may contribute to conduction block and the initiation of triggered reentrant activity. The dynamic gap junction model represents a realistic tool for further investigation of the role of cardiac g_j in numerical simulations of action potential propagation and arrhythmogenesis.

Acknowledgments

We thank Dr. David Cameron, Dept of Neuroscience and Physiology, and the laboratory of Dr. Paul Massa, especially Charlene Wu, Dept. of Neurology, SUNY Upstate Medical University, for the contributions to this study.

Grants: This work was supported, in part, by National Heart, Lung, and Blood Institute Grants HL-42220 (to R. D. Veenstra) and HL-45466 (to E. C. Beyer and R. D. Veenstra).

Appendix

Appendix

The time-dependent decay of I_j was modeled with the following expressions:

$$G_1^{t+1} = \left(G_1^t - G_{\min 1}\right) \cdot \left\{1 - \mathrm{d}t \cdot A_1 \cdot \exp\left[\left(V_j^{t+1} - 40\right)/V_{\tau 1}\right]\right\} + G_{\min 1} \tag{4}$$

and

$$G_2^{t+1} = \left(G_2^t - G_{\min 2}\right) \cdot \left\{1 - \mathrm{d}t \cdot A_2 \cdot \exp\left[\left(V_j^{t+1} - 40\right)/V_{\tau 2}\right]\right\} + G_{\min 2} \tag{5}$$

where $G_{\min 1} = G_{\min 2}$. The initial conditions for each inactivation component were defined by

$$G_1^{t=0} = G_1^0 = G_{\max 1} + G_{\min 1} \tag{6}$$

and

$$G_2^{t=0} = G_2^0 = G_{\max 2} + G_{\min 2} \tag{7}$$

where

$$G_{\max 1} + G_{\max 2} + G_{\min 1} + G_{\min 2} = 1 \tag{8}$$

The V_j-dependent time constants were computed based on the exponential decay time constants described in Fig. 5B. The faster inactivation component, G_1^{t+1}, was assigned a rate six times greater than the slower inactivation component (G_2^{t+1}) in accordance with the two fitted time components of the CL-dependent G_j curves. G_2^t was assigned the initial value of A^0 (=0.00148 ms^{-1}) at 40 mV in accordance with Eq. 3. To calculate the degree of inactivation during each successive action potential, the following conditions were assessed for each time step:

$$\text{IF } \left[V_j^{t-1} > 1\ \text{mV}\right], \text{THEN } G_1^t = \text{Eq.4 and } G_2^t = \text{Eq.5, ELSE } G_1^t = \text{Eq.6 and } G_2^t = \text{Eq.7} \tag{L1}$$

This logic statement ensures that inactivation is removed once V_j has returned to resting levels and will commence again when V_j increases above a certain threshold value according to the computed V_j-dependent inactivation time constants.

The increase in G_j observed during the ventricular action potential was modeled according to the following expressions:

$$R_1^{t+1} = A_{R1} \cdot \exp\left(V_j^{t+1}/V_{R1}\right) \tag{9a}$$

and

$$R_2^{t+1} = A_{R2} \cdot \exp\left(V_j^{t+1}/V_{R2}\right) \tag{10}$$

To model the changes in the recovery process that occurred during prolonged repolarization, the amplitude (A_{R1}) and voltage constant (V_{R1}) of Eq. 9a were varied to best fit the data. Plots of the A_{R1} and V_{R1} values from Table 3 relative to the time step for the repolarization voltage changes (dt) revealed that A_{R1} is an exponential function of dt, whereas V_{R1} varied linearly. The exact solutions were:

$$A_{R1} = -0.385 \pm 0.042 \cdot \exp\left(dt/1.01 \pm 0.30\right) + 0.72 \pm 0.03 \tag{9b}$$

and

$$V_{R1} = 3.20 \pm 0.3 \cdot dt + 19.3 \pm 0.8. \tag{9c}$$

These functions can be substituted into Eq. 9a to provide continuous solutions to the early recovery process during changes in the rate of repolarization expressed as a percentage change from control conditions as follows:

$$R_1^{t+1} = \left[-0.385 \cdot \exp\left(dt/1.01\right) + 0.72\right] \cdot \exp\left[V_j^{t+1}/(3.2 \cdot dt + 19.3)\right] \tag{9d}$$

To ensure that the V_j-dependent recovery process occurred only when V_j was decreasing, the following logic statement was invoked:

$$\text{AND}\left[V_j^{t+1} > 1\ \text{mV},\ V_j^{t+1} < V_j^t\right], R_j^{t+1} = \text{Eq.9}a\ (\text{or}\ d)\ \text{and}\ R_2^t = \text{Eq.10}. \tag{L2}$$

If the output of this logic statement was false, then Eqs. 9 and 10 were multiplied times zero.

The time-dependent value of

$$G_j^{t+1} = (L1 \cdot \text{Eq.4}) + (L1 \cdot \text{Eq.5}) + [L2 \cdot \text{Eq.9}a\ (\text{or}\ d)] + (L2 \cdot \text{Eq.10}) \tag{11}$$

Again, the threshold V_j value for resetting Eqs. 4, 5, 9, and 10 to the initial conditions was chosen to eliminate the instability (noise) of the mathematical solutions to the expressions as

the $\lim V_j^{t+1} \to 0$. All solutions to Eq. 11 corresponding to the experimental data are graphically illustrated in Fig. 7 and listed in Tables 2 and 3.

References

1. Alcoléa S, Théveniau-Ruissy M, Jarry-Ruchard T, Marics I, Tzouanacou E, Chauvin JP, Briand JP, Moorman AF, Lamers WH, Gros DB. Downregulation of connexin 45 gene products during mouse heart development. Circ Res 1999;84:1365–1379. [PubMed: 10381888]
2. Bastide B, Neyses L, Ganten D, Paul M, Willecke K, Traub O. Gap junction protein connexin40 is preferentially expressed in vascular endothelium and conductive bundles of rat myocardium and is increased under hypertensive conditions. Circ Res 1993;73:1138–1149. [PubMed: 8222085]
3. Beyer EC. Molecular cloning and developmental expression of two chick embryo gap junction proteins. J Biol Chem 1990;265:14439–14443. [PubMed: 2167316]
4. Bradford MM. A rapid and sensitive method for the quantitation of microgram quantities of protein using the principle of protein-dye binding. Anal Biochem 1976;72:248–254. [PubMed: 942051]
5. Cooklin M, Wallis WRJ, Sheridan DJ, Fry CH. Changes in cell-to-cell electrical coupling associated with left ventricular hypertrophy. Circ Res 1997;80:765–771. [PubMed: 9168778]
6. Coppen SR, Dupont E, Rothery S, Severs NJ. Connexin45 expression is preferentially associated with the ventricular conduction system in the embryonic and mature rodent heart. Circ Res 1998;82:232–243. [PubMed: 9468194]
7. Coppen SR, Severs NJ, Gourdie RG. Connexin 45 (α6) expression delineates an extended conduction system in the embryonic and mature rodent heart. Dev Genet 1999;24:82–90. [PubMed: 10079513]
8. Gemel J, Valiunas V, Brink PR, Beyer EC. Connexin43 and connexin26 form gap junctions, but not heteromeric channels in co-expressing cells. J Cell Sci 2004;117:2469–2480. [PubMed: 15128867]
9. Giepmans BN, Moolenar WH. The gap junction protein connexin43 interacts with the second PDZ domain of the zona occludens-1 protein. Curr Biol 1998;8:931–934. [PubMed: 9707407]
10. Gourdie RG, Severs NJ, Green CR, Rothery S, Germroth P, Thompson RP. The spatial distribution and relative abundance of gap-junctional connexin40 and connexin43 correlate to functional properties of components of the cardiac atrioventricular conduction system. J Cell Sci 1993;105:985–991. [PubMed: 8227219]
11. Gros D, Jarry-Guichard T, Ten Velde I, de Maziere A, van Kempen MJ, Davoust J, Briand JP, Moorman AF, Jongsma HJ. Restricted distribution of connexin40, a gap junction protein, in mammalian heart. Circ Res 1994;74:839–851. [PubMed: 8156631]
12. Hennemann H, Suchyna T, Lichten-Fraté H, Jungbluth S, Dahl E, Schwarz J, Nicholson BJ, Willecke K. Molecular cloning and functional expression of mouse connexin40, a second gap junction gene preferentially expressed in lung. J Cell Biol 1992;117:1299–1310. [PubMed: 1318884]
13. Henriquez AP, Vogel R, Muller-Borer BJ, Henriquez CS, Weingart R, Cascio W. Influence of dynamic gap junction resistance on impulse propagation in ventricular myocardium: a computer simulation study. Biophys J 2001;81:2112–2121. [PubMed: 11566782]
14. Johnson CM, Kanter EM, Green KG, Laing JG, Betsuyaku T, Beyer EC, Steinberg TH, Saffitz JE, Yamada KA. Redistribution of connexin45 in gap junctions of connexin43-deficient hearts. Cardiovasc Res 2002;53:921–935. [PubMed: 11922902]
15. Kanter EM, Laing JG, Beau SL, Beyer EC, Saffitz JE. Distinct patterns of connexin expression in canine Purkinje fibers and ventricular muscle. Circ Res 1993;72:1124–1131. [PubMed: 8386597]
16. Kanter HL, Saffitz JE, Beyer EC. Cardiac myocytes express multiple gap junction proteins. Circ Res 1992;70:438–444. [PubMed: 1310450]
17. Kléber AG, Riegger CB, Janse MJ. Electrical uncoupling and increase of extracellular resistance after induction of ischemia in isolated, arterially perfused rabbit papillary muscle. Circ Res 1987;67:271–279.
18. Kléber AG, Rudy Y. Basic mechanisms of cardiac impulse propagation and associated arrhythmias. Physiol Rev 2004;84:431–488. [PubMed: 15044680]
19. Kumar R, Joyner RW. An experimental model of the production of early after depolarizations by injury current from an ischemic region. Pflügers Arch 1994;428:425–32.

20. Kwong KF, Schuessler RB, Green KG, Laing JG, Beyer EC, Boineau JP, Saffitz JE. Differential expression of gap junction proteins in the canine sinus node. Circ Res 1998;82:604–612. [PubMed: 9529165]
21. Lin X, Crye M, Veenstra RD. Regulation of connexin43 gap junctional conductance by ventricular action potentials. Circ Res 2003;93:e63–e73. [PubMed: 12946947]
22. Lin X, Veenstra RD. Action potential modulation of connexin40 gap junctional condutance. Am J Physiol Heart Circ Physiol 2004;286:H1726–H1735. [PubMed: 14693688]
23. Luke RA, Saffitz JE. Remodeling of ventricular conduction pathways in healed canine infarct border zones. J Clin Invest 1991;87:736–754.
24. Luo CH, Rudy Y. A dynamic model of the cardiac ventricular action potential. I. Simulations of ionic currents and concentration changes. Circ Res 1994;74:1071–1096. [PubMed: 7514509]
25. Moreno AP, Fishman GI, Spray DC. Phosphorylation shifts the unitary conductance and modifies voltage-dependent kinetics of human connexin43 gap junction protein channels. Biophys J 1992;62:51–53. [PubMed: 1376174]
26. Peters NS, Coromilas J, Severs NJ, Wit AL. Disturbed connexin43 gap junction distribution correlates with the location of reentrant circuits in the epicardial border zone of healing canine infarcts that cause ventricular tachycardia. Circulation 1997;95:988–996. [PubMed: 9054762]
27. Peters NS, Green CR, Poole-Wilson PA, Severs NJ. Reduced content of connexin43 in ventricular myocardium from hypertrophied and ischemic human hearts. Circulation 1993;88:864–875. [PubMed: 8394786]
28. Petrecca K, Amellal F, Laird DW, Cohen SA, Shrier A. Sodium channel distribution within the rabbit atrioventricular node as analyzed by confocal microscopy. J Physiol 1997;501:263–274. [PubMed: 9192299]
29. Poelzing S, Akar FG, Baron E, Rosenbaum DS. Heterogeneous connexin43 expression produces electrophysiological heterogeneities across ventricular wall. Am J Physiol Heart Circ Physiol 2004;286:H2001–H2009. [PubMed: 14704225]
30. Rudy, Y. The Handbook of Physiology. The Cardiovascular System. The Heart. Bethesda, MD: Am. Physiol. Soc.; 2002. The cardiac ventricular action potential; p. 531-547.sect. 2, vol. I, Chap. 13
31. Sáez JC, Berthoud VM, Brañes MC, Martínez AD, Beyer EC. Plasma membrane channels formed by connexins: their regulation and function. Physiol Rev 2003;83:1359–1400. [PubMed: 14506308]
32. Saiz J, Ferrero JM Jr, Monserrat M, Ferraro JM, Thakor NV. Influence of electrical coupling on early afterdepolarizations in ventricular myocytes. IEEE Trans Biomed Eng 1999;46:138–147. [PubMed: 9932335]
33. Schram G, Pourrier M, Melnyk P, Nattel S. Differential distribution of cardiac ion channel expression as a basis for regional specialization in electrical function. Circ Res 2002;90:939–950. [PubMed: 12016259]
34. Shaw RM, Rudy Y. The vulnerable window for unidirectional block in cardiac tissue: characterization and dependence on membrane excitability and intercellular coupling. J Cardiovasc Electrophysiol 1995;6:115–131. [PubMed: 7780627]
35. Takens-Kwak BR, Jongsma HJ. Three distinct channel conductances and their modulation by phosphorylation treatment. Pflügers Arch 1992;422:198–200.
36. Toyofuku T, Yabuki M, Otsu K, Kuzuya T, Tada T, Hori M. Direct association of the gap junction protein connexin-43 with ZO-1 in cardiac myocytes. J Biol Chem 1998;273:12725–12731. [PubMed: 9582296]
37. Traub O, Eckert R, Lichten-Fraté H, Elfgang C, Bastide B, Scheidtmann KH, Hülser DF, Willecke K. Immunochemical and electrophysiological characterization of murine connexin40 and -43 in mouse tissues and transfected human cells. Eur J Cell Biol 1994;64:101–112. [PubMed: 7957300]
38. Van Veen TAB, van Rigen HVM, Opthof T. Cardiac gap junction channels: modulation of expression and channel properties. Cardiovasc Res 2001;51:217–229. [PubMed: 11470461]
39. Veenstra RD. Developmental changes in regulation of embryonic chick heart gap junctions. J Membr Biol 1991;119:253–265. [PubMed: 1711582]
40. Veenstra RD. Voltage clamp limitations of dual whole cell recordings of gap junction current and voltage recordings. I. Conductance measurements. Biophys J 2001;80:2231–2247. [PubMed: 11325726]

41. Vogel R, Weingart R. Mathematical model of vertebrate gap junctions derived from electrical measurements of homotypic and heterotypic channels. J Physiol 1998;501:177–189. [PubMed: 9625876]

42. Yao JA, Gutstein DE, Liu F, Fishman GI, Wit AL. Cell coupling between ventricular myocyte pairs from connexin43-deficient murine hearts. Circ Res 2003a;93:736–743. [PubMed: 14500334]

43. Yao JA, Hussain W, Patel P, Peters NS, Boyden PA, Wit AL. Remodeling of gap junctional channel function in epicardial border zone of healing canine infarcts. Circ Res 2003b;92:437–443. [PubMed: 12600896]

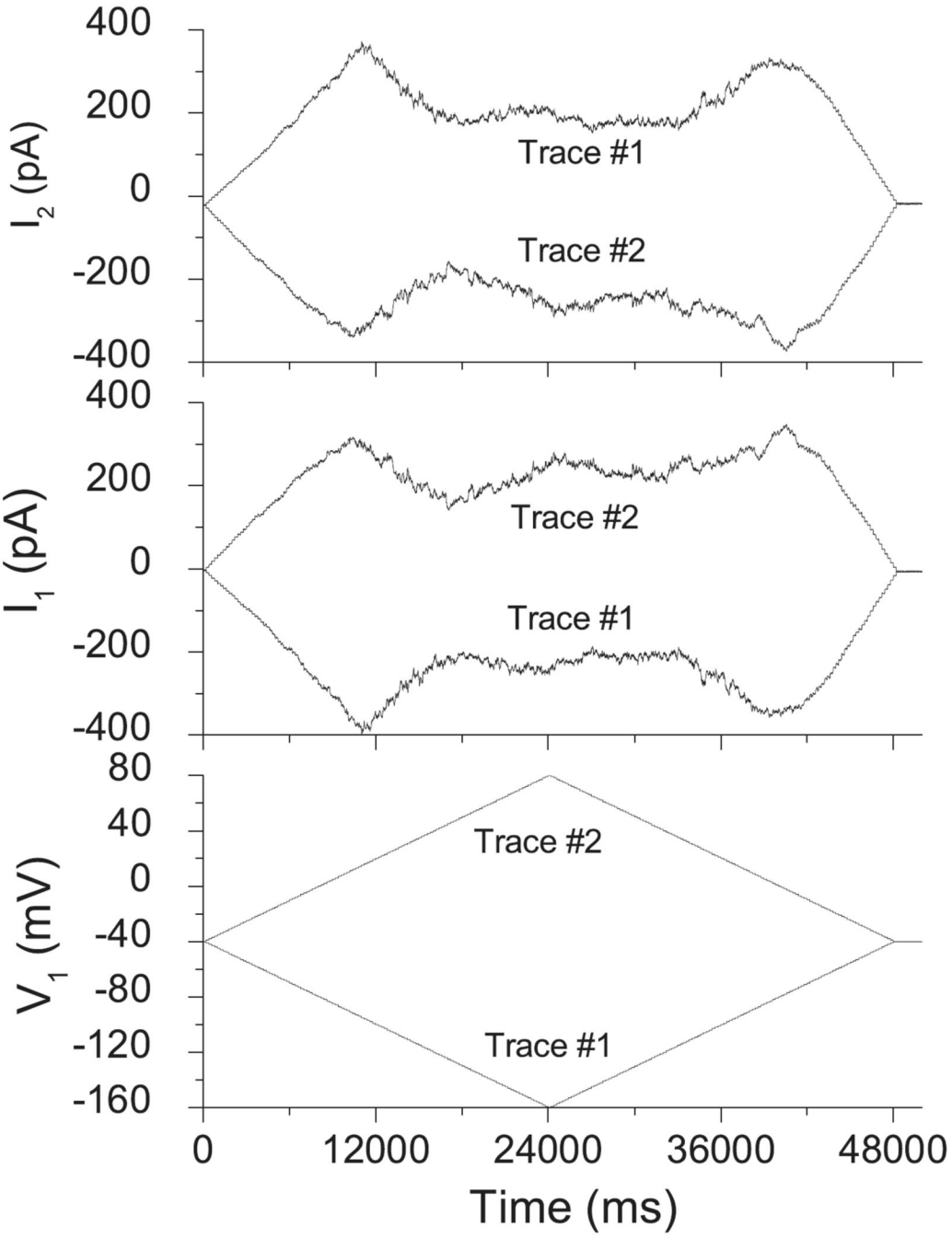

Fig. 1.

Voltage-clamp protocol for steady-state inactivation and recovery curves. The whole cell currents representing the negative junctional current signal (*top*) and the whole cell currents and command voltages for the partner cell (*middle* and *bottom*) during one run of the 200 ms/mV, ± 120-mV voltage ramp applied to ventricular myocytes are shown. The linear slope of the current (*I*)-voltage (*V*) relationship at low voltages was used to normalize the data from different experiments. The linear slope conductances from 0 to ±20 mV were 6.20 and 6.95 nS for *traces 1* and *2* during the rising phase of the transjunctional voltage (V_j) ramp and were 10.50 and 10.30 nS during the returning phase, indicative of a facilitation of junctional conductance (g_j) during the recovery process.

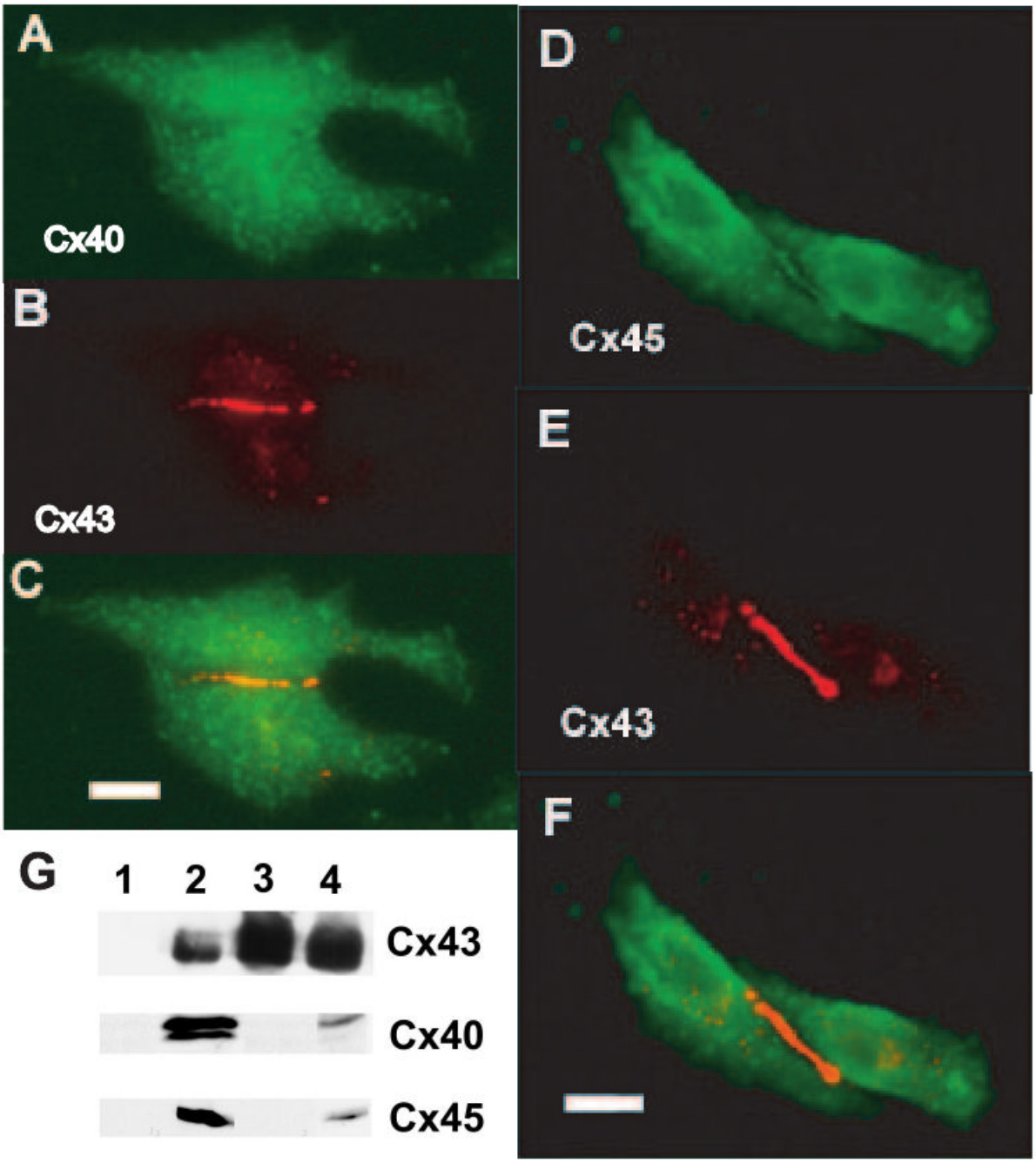

Fig. 2.

Fluorescent immunolocalization of endogenous murine connexin (Cx) expression. Immunohistochemical localization of endogenous Cx40 (*A*), Cx45 (*D*), or Cx43 (*B* and *E*) expression and colocalization of Cx40 with Cx43 (*C*) or Cx45 (*F*) in paired ventricular myocytes after 2 days in culture are shown. Only trace amounts of Cx40 and Cx45 are evident in neonatal murine ventricular myocytes cultured at low density for 48 h to mimic experimental electrophysiological conditions. Negative controls without overnight incubation with the specific Cx antibody revealed negligible background fluorescence (data not shown). *G*: immunoblot analysis of Cx43, Cx40, and Cx45 in cultured cells or fresh frozen ventricular tissue from neonatal mice. Whole cell lysates were loaded in the following order: *lane 1*, N2a

untransfected cells (for Cx43 detection 10 μg protein, for Cx40 or Cx45 detection 100 μg protein); *lane 2*, Cx-expressing cells (for Cx43 detection 10 μ*g* protein from N2a cells stably transfected with rat Cx43; for Cx40 detection 100 μg protein from N2a cells stably transfected with rat Cx40; for Cx45 detection 200 μg protein from HEK293 cells); *lane 3*, cultured ventricular myocytes (for Cx43 detection 10 μg protein, for Cx40 or Cx45 detection 50 μg protein); *lane 4*, ventricular tissue from neonatal mice (for Cx43 detection 10 μg protein; for Cx40 or Cx45 detection 100 μg protein). Samples were resolved by SDS-PAGE, transferred to membranes, and blotted with anticonnexin antibodies as described in Materials and Methods.

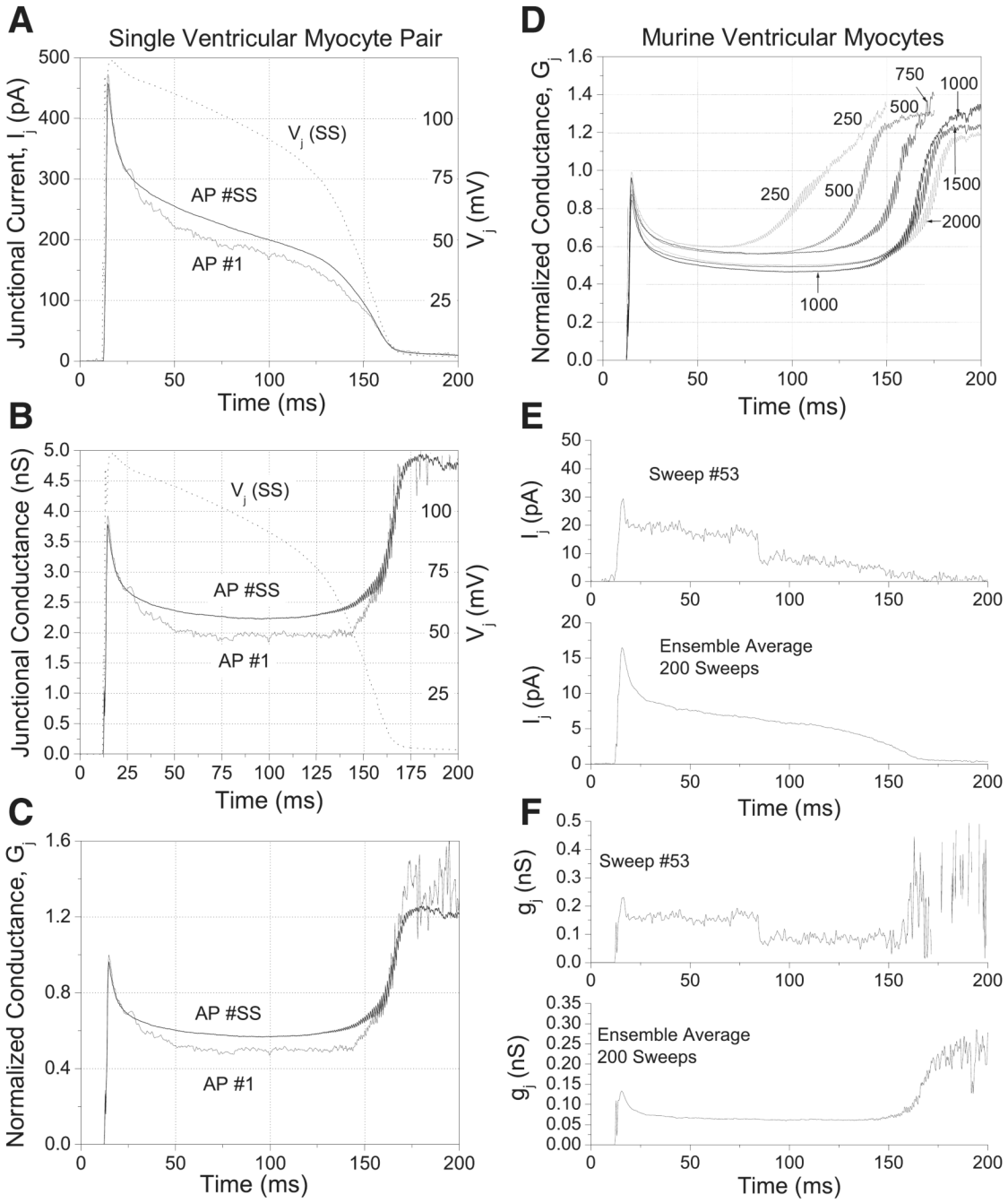

Fig. 3.

Junctional currents and conductance during the ventricular action potential. *A*: junctional current (I_j) recorded as $-\Delta I_2$ during application of the ventricular action potential for the first beat (AP #1) and the average of the last 100 beats (AP #SS) at a rate of 1 beat/s for 200 s. *B*: calculated g_j during this same experiment using the actual applied V_j (Eq. 1, see Materials and Methods). *C*: normalized g_j from 7 experiments. The g_j was normalized to the peak value of g_j for each ventricular myocyte cell pair during the train of 200 action potentials. *D: G_j* values of ventricular cardiac gap junctions after pacing at 6 different cycle lengths (CL) of stimulation. On average, g_j inactivates by 40–50% and recovers completely during *phase 3* and *phase 4* of the action potential. Some facilitation (increase in g_j above peak values) of g_j is evident in

ventricular myocytes during the late phases of repolarization. *E*: single sweep depicting single gap junction channel responses to the ventricular action potential. The averaged I_j trace from all 200 sweeps closely resembles the macroscopic recordings shown in *C*. *F*: corresponding g_j calculations for the I_j traces shown in *E*. This indicates that the basis for the time-dependent changes in g_j during the action potential are the result of the V_j-dependent gating of individual gap junction channels.

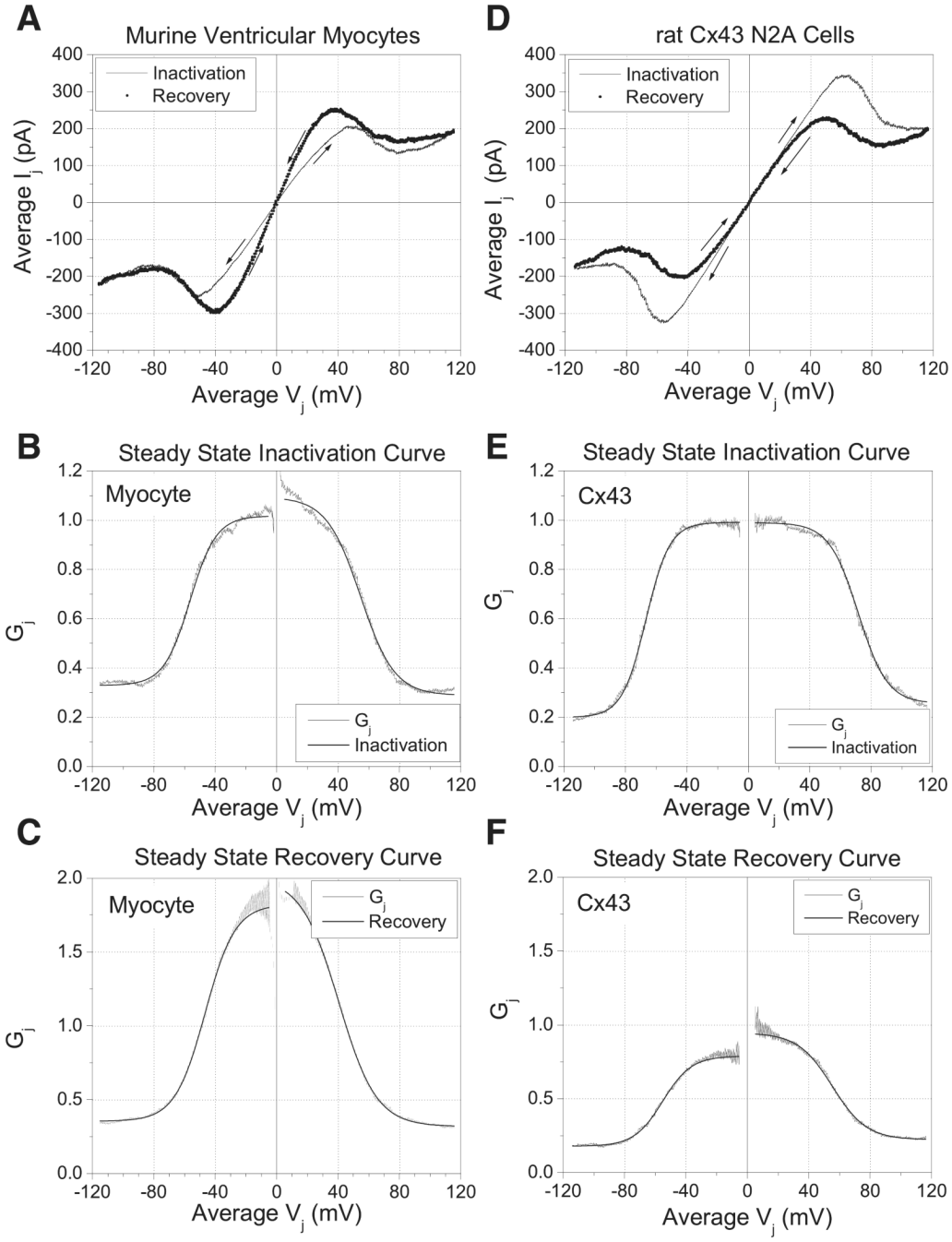

Fig. 4.

Steady-state V_j-dependent inactivation and recovery conductance curves. *A* and *D*: average I_j in response to a ±120 mV, 200 ms/mV V_j ramp during the increasing and decreasing V_j phases for ventricular myocyte (*A*) and Cx43-N2a (*D*) cell gap junctions. *B* and *E*: steady-state G_j-V_j ventricular myocyte (*B*) and Cx43 (*E*) curves during the inactivation (increasing V_j) phase of the V_j ramp. *C* and *F*: steady-state G_j-V_j curves for ventricular myocytes (*C*) and Cx43 (*F*) gap junctions during the recovery (decreasing V_j) phase do not follow the same path as inactivation. The Boltzmann curves (solid line) for each were determined using Eq. 2 (see Materials and Methods). The parameter values are provided in Table 1.

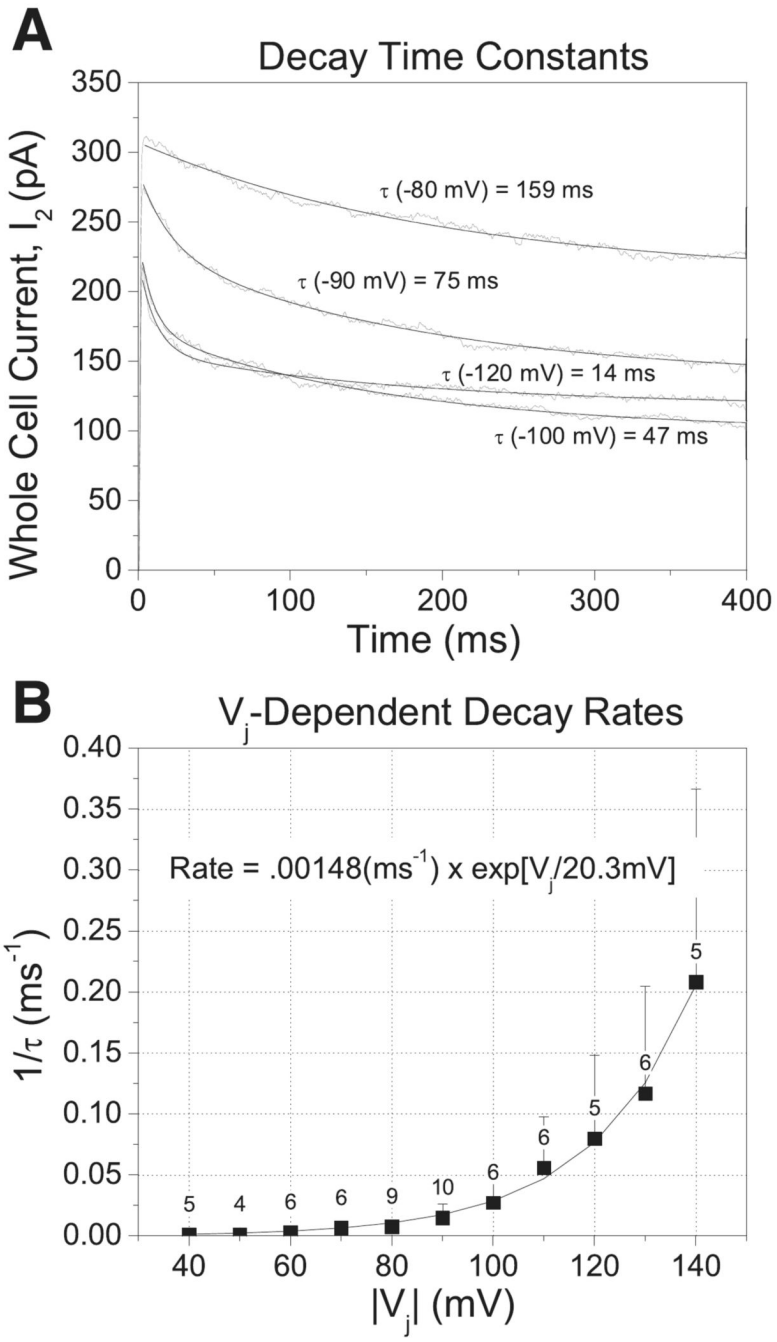

Fig. 5.

V_j-dependent kinetics of ventricular G_j inactivation. *A*: unsubtracted whole cell currents during a voltage clamp step to the indicated V_j value from a single ventricular myocyte cell pair. The displayed current traces are the ensemble average of 5 V_j pulses. The decay time constants (τ_{decay}) were determined from exponential fits of the first second of the 2.5-s duration pulse. *B*: inactivation rate ($1/\tau_{decay}$) was plotted as a function of V_j for *N* experiments (indicated in parentheses). The exponential fit of the rate constants reveals an *e*-fold increase in the rate of inactivation for every 20.3-mV increase in V_j.

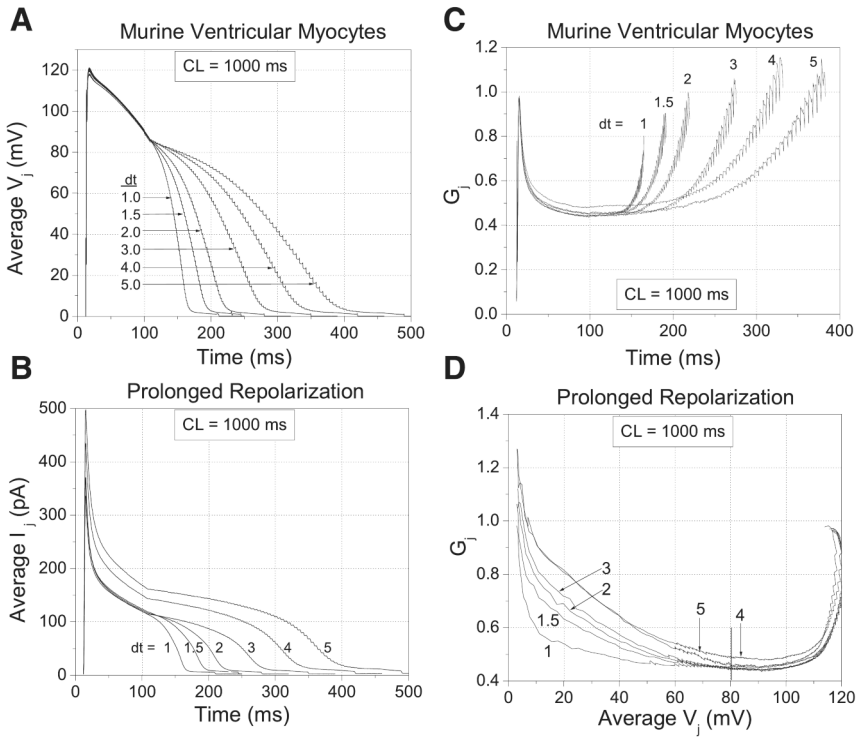

Fig. 6.

Effect of prolonged repolarization on the recovery process of ventricular G_j. *A*: average V_j from 7 experiments indicating the extension of the repolarization phase of the CL = 1,000 ms ventricular action potential by increasing the time step (*dt*) from 1 to 5 ms, as indicated. *B*: average I_j from the same experiments in response to a train of 20 action potentials/experiment. *C*: time-dependent G_j curves for the same experiments. *D*: same G_j curves as in *C* plotted as a function of V_j, as depicted in *A*. G_j increases with increasing *dt* during phase 3 and 4 repolarization. There is no evidence for a V_j-dependent recovery time constant, since the different curves demonstrate convergence toward the *dt* = 5 ms curve at all voltages.

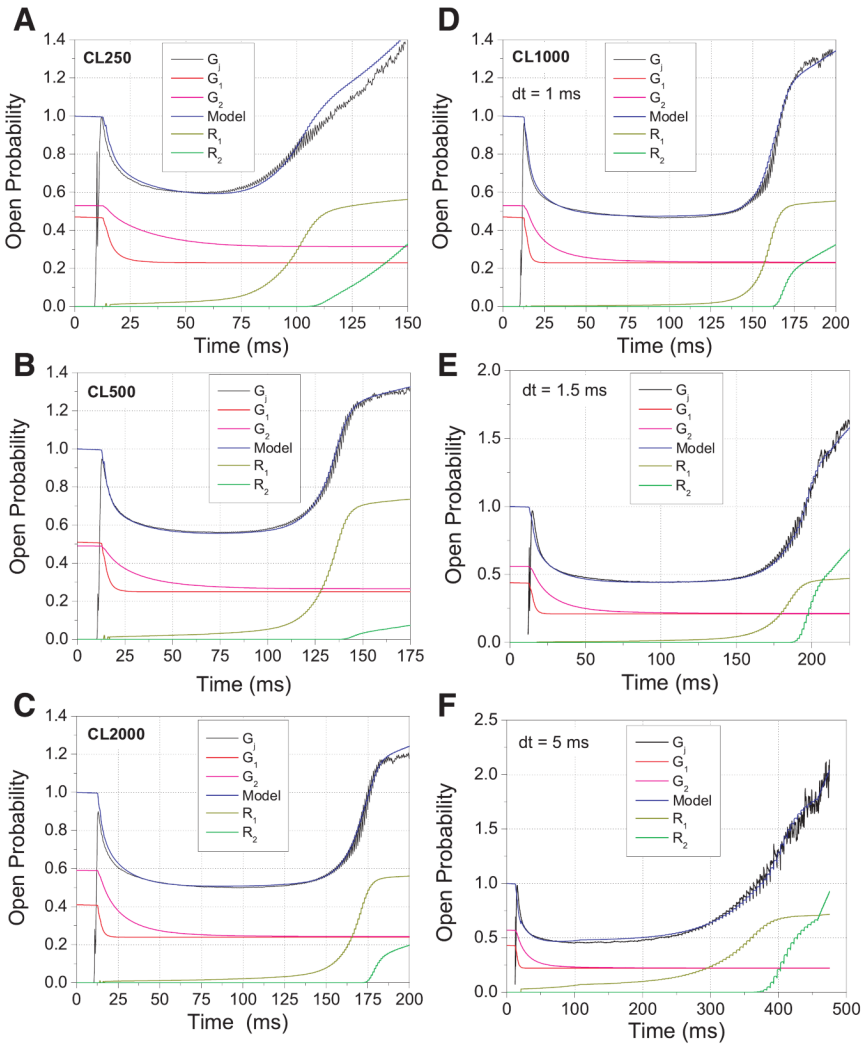

Fig. 7.

Model of ventricular G_j at different cycle lengths of stimulation and rates of repolarization. The average time-dependent G_j curve at each CL, as shown in Fig. 3D, was modeled according to Eq. 11 (see Appendix) for 250 (*A*), 500 (*B*), 2,000 (*C*), and 1,000 (*D*) ms CL. Parameter values for Eqs. 4, 5, 9, and 10 used to define the 2 inactivation (G_1^{t+1} and G_2^{t+1}) and recovery (R_1^{t+1} and R_2^{t+1}) components (see Appendix) are provided in Table 2. The average time-dependent G_j curves shown in Fig. 6C were modeled using Eq. 11, and the results are displayed graphically for the 1.5-ms (*E*) and 5.0-ms (*F*) *dt* applied to *phase 3* and early *phase 4* of the CL = 1,000 ms ventricular action potential. The values of the individual inactivation and recovery components for all *dt* intervals are listed in Table 3.

Table 1
Steady-state junctional conductance inactivation and recovery curves

	Ventricular Myocytes (n = 4)		N2a-Cx43 Cells (n = 6)	
	$-V_j$	$+V_j$	$-V_j$	$+V_j$
	Inactivation parameter			
G_{max}	1.00±0.001	1.04±0.002	0.99±0.001	0.99±0.001
G_{min}	0.31 ±0.001	0.37±0.001	0.20±0.001	0.26±0.001
$V_{1/2}$, mV	−57.06±0.04	+55.87±0.09	−66.78±0.04	+71.61 ±0.07
Valence	−3.48±0.02	+3.06±0.03	−3.25±0.02	+2.66±0.02
	Recovery parameter			
G_{max}	1.60±0.002	2.46±0.005	0.79±0.001	0.95±0.001
G_{min}	0.30±0.001	0.43±0.002	0.18±0.001	0.22±0.001
$V_{1/2}$, mV	−43.36±0.06	+44.78±0.09	−55.17±0.07	+55.35±0.10
Valence	−2.35±0.01	+2.09±0.01	−2.72±0.02	+2.27±0.02

Values are means ± SE; n, no. of experiments. G_{max}, maximum conductance; G_{min}, minimum conductance; $V_{1/2}$, half-maximal voltage; V_j, transjunctional voltage; –, negative V_j; +, positive V_j.

Table 2

Frequency dependence of ventricular junctional conductance

Parameter	Cycle Length, ms					
	250 (*n* = 7)	**500 (*n* = 3)**	**750 (*n* = 6)**	**1,000 (*n* = 7)**	**1,500 (*n* = 4)**	**2,000 (*n* = 5)**
G_{max1}	0.24	0.26	0.18	0.24	0.22	0.17
G_{min1}	0.23	0.25	0.27	0.23	0.24	0.24
G_{max2}	0.30	0.24	0.28	0.30	0.30	0.35
G_{min2}	0.23	0.25	0.27	0.23	0.24	0.24
A_1	0.00888	0.00888	0.00888	0.00888	0.00888	0.00888
$V_{\tau 1}$, mV	20.3	20.3	20.3	20.3	20.3	20.3
A_2	0.00148	0.00148	0.00148	0.00148	0.00148	0.00148
$V_{\tau 2}$, mV	20.3	20.3	20.3	20.3	20.3	20.3
A_{R1}	0.60	0.80	0.60	0.60	0.60	0.60
V_{R1}, mV	27.0	28.0	26.0	22.0	24.0	28.0
A_{R2}	1.05	0.35	1.40	1.05	1.05	0.70
V_{R2}, mV	1.50	1.50	1.50	1.50	1.50	1.50

$A_{(1 \text{ or } 2)}$, amplitude; *V*, voltage. *n*, No. of experiments. See the Appendix for parameter definitions.

Table 3

Effect of prolonged repolarization on ventricular junctional conductance

	Time Step, ms					
Parameter	**1**	**1.5**	**2**	**3**	**4**	**5**
G_{max1}	0.21	0.23	0.23	0.23	0.19	0.21
G_{min1}	0.22	0.21	0.21	0.21	0.23	0.22
G_{max2}	0.35	0.35	0.35	0.35	0.35	0.35
G_{min2}	0.22	0.21	0.21	0.21	0.21	0.22
A_1	0.00888	0.00888	0.00888	0.00888	0.00888	0.00888
$V_{\tau 1}$, mV	20.3	20.3	20.3	20.3	20.3	20.3
A_2	0.00148	0.00148	0.00148	0.00148	0.00148	0.00148
$V_{\tau 2}$, mV	20.3	20.3	20.3	20.3	20.3	20.3
A_{R1}	0.32	0.5	0.60	0.60	0.70	0.74
V_{R1}, mV	21.0	25.2	28.2	26.6	31.4	36.2
A_{R2}	2.45	1.90	2.10	2.10	2.10	2.10
V_{R2}, mV	1.5	1.5	1.5	1.5	1.5	1.5